

# MEASUREMENT OF SARCOMERE SHORTENING IN SKINNED FIBERS FROM FROG MUSCLE BY WHITE LIGHT DIFFRACTION

YALE E. GOLDMAN

*Department of Physiology, University of Pennsylvania School of Medicine, Philadelphia, Pennsylvania 19104-6085*

**ABSTRACT** A new optical-electronic method has been developed to detect striation spacing of single muscle fibers. The technique avoids Bragg-angle and interference-fringe effects associated with laser light diffraction by using polychromatic (white) light. The light is diffracted once by an acousto-optical device and then diffracted again by the muscle fiber. The double diffraction reverses the chromatic dispersion normally obtained with polychromatic light. In frog skinned muscle fibers, active and passive sarcomere shortening were smooth when observed by white light diffraction, whereas steps and pauses occurred in the striation spacing signals obtained with laser illumination. During active contractions skinned fibers shortened at high rates ( $3\text{--}5\ \mu\text{m/s}$  per half sarcomere,  $0\text{--}5^\circ\text{C}$ ) at loads below 5% of isometric tension. Compression of the myofibrillar lateral filament spacing using osmotic agents reduced the shortening velocity at low loads. A hypothesis is presented that high shortening velocities are observed with skinned muscle fibers because the cross-bridges cannot support compressive loads when the filament lattice is swollen.

## INTRODUCTION

Studies of the mechanical kinetics of muscle contraction require measurement of sarcomere length to indicate or control filament sliding. Since connections to the ends of a muscle preparation generally introduce compliance in series with the sarcomeres, several methods have been developed to record segment length or sarcomere length away from the end compliance. Photography and cinephotography can achieve this purpose (Huxley and Peachey, 1961; Moss, 1979; Julian and Moss, 1980; Julian et al., 1986) but are not appropriate for feedback control during a contraction.

For intact single fiber studies, Gordon et al. (1966) developed a "spot follower" system, which electronically detected the spacing between foil markers attached to the fiber. For studies of skinned muscle fibers, Goldman and Simmons (1984) found that uneven contraction developed near the attached markers, preventing them from adopting the spot follower technique.

A laser diffraction instrument was developed to monitor striation spacing for feedback control during isometric transients (Goldman and Simmons, 1984, 1986) and for measuring force-velocity curves (Ferenczi et al., 1984). At the spacial resolution of several nanometers per half sarcomere, the laser diffraction instrument produced erroneous

signals unless the incident angle of the laser beam at the fiber was oscillated sinusoidally. This procedure limited the bandwidth and signal-to-noise ratio of the instrument (Goldman and Simmons, 1984). The results suggested that laser diffraction by a muscle was complicated by the relative thickness of a single fiber ( $50\text{--}200\ \mu\text{m}$ ) in comparison to the wavelength of the light ( $0.63\ \mu\text{m}$  in air;  $0.46\ \mu\text{m}$  within the fiber). In a diffraction experiment, constructive interference of rays scattered from different depths within a thick specimen depends on both the spacing and the tilt of the lattice planes (Bragg, 1933). This Bragg-angle phenomenon may cause errors in laser diffraction measurements of striation spacing (Rüdel and Zite-Ferenczy, 1979, 1980; Goldman and Simmons, 1984).

A possible method to circumvent these difficulties is to monitor sarcomere length by polychromatic light scattering. Each color has a different Bragg-angle and thus groups of myofibrils with a range of azimuthal tilt angles would be represented in the diffracted light. With polychromatic (white) light, diffraction introduces chromatic dispersion, i.e., it produces a spectrum in the diffraction plane. Therefore, special optical arrangements are necessary to detect the diffraction angle accurately. In the present work, a second diffraction by a variable-spacing phase grating, an acousto-optical deflector, was used to reverse the chromatic dispersion. The instrument produces a high time and spacial resolution sarcomere length signal from a central segment of the fiber.

The white light diffraction instrument has been used to

---

Address Correspondence to Dr. Y. E. Goldman, Department of Physiology, School of Medicine, University of Pennsylvania, Philadelphia, PA 19104-6085.

study the force-velocity curve of frog skinned muscle fibers. Maximum sarcomere shortening velocity ( $V_{\max}$ ) was found to be higher than values published for intact fibers. Osmotic agents (dextran T-500 or polyvinylpyrrolidone) reduced  $V_{\max}$ , leading to the hypothesis that  $V_{\max}$  depends on the lateral filament spacing of the myofibrillar lattice. The equipment was also used to investigate some artifacts of the laser light diffraction method. A preliminary report of these findings was presented to the Biophysical Society (Goldman, 1983). The instrument has also been applied in other studies from this laboratory (Goldman et al., 1984; Dantzig and Goldman, 1985).

## METHODS

### Muscle Fiber Procedures

Skinned muscle fibers were prepared from *Rana temporaria* obtained from Ireland and stored at 4°C for 2 wk to several months. Single semitendinosus fibers were isolated and the surface membrane was removed by mechanical dissection. Skinned fibers were mounted in aluminum clips between a force transducer and length step motor and fiber dimensions were measured by compound microscopy as described by Goldman and Simmons (1984).

The solutions for relaxing and activating the fibers had 5 mM MgATP, 1 mM free  $Mg^{2+}$ , and 30 mM total EGTA. Free  $Ca^{2+}$  concentrations were calculated assuming an apparent association constant for  $Ca^{2+}$  and EGTA of  $K_{app} = 10^{6.47}$ . Rigor solution had 34 mM EDTA, and no added ATP or Mg. All solutions had 100 mM TES buffer, 200 mM ionic strength, pH 7.1 at 0°C. Linear synthetic polymers, polyvinylpyrrolidone (PVP-40, Fluka AG, Buchs, Switzerland) and dextran T-500 (Pharmacia Fine Chemicals, Piscataway, NJ) were added to the solutions in some experiments to osmotically compress the myofilament lattice. An acidic impurity in the PVP-40 stock was removed by ultrafiltration. Further details on preparation of the solutions are given in Goldman and Simmons (1984) and Matsubara et al. (1984).

The experimental trough had a volume of 320  $\mu$ l and was exchanged by evacuating the solution with the fiber in place and then filling the trough with a new solution. The contents of the trough were continuously stirred by repeatedly injecting and extracting  $\sim 10$   $\mu$ l of the solution with a reciprocating syringe. Temperature was maintained at 0–5°C by circulating a cold ethylene glycol/water mixture through anodized aluminum sides of the trough.

For shortening velocity measurements an isotonic tension level was set by a tension normalizer circuit similar to that described by Ferenczi et al. (1984). The cycling procedure of Brenner (1983) was used to obtain repeated isotonic shortening records during a single incubation in activating solution and to improve the uniformity of the striations. However, with skinned frog fibers the diffraction pattern became too diffuse at full activation for operation of the striation spacing device, so the experiments on actively contracting fibers were limited to  $Ca^{2+}$  concentrations leading to 30–80% activation.

### White Light Diffraction Technique

*Principle of the Method.* Light diffraction by a grating with constant spacing obeys the grating equation

$$\sin(\theta_d) = k\lambda/d - \sin(\theta_i), \quad (1)$$

where  $\theta_i$  and  $\theta_d$  are meridional angles of the incident and diffracted beams, respectively,  $k$  is the diffraction order,  $\lambda$  is the wavelength of the irradiation, and  $d$  is the grating spacing.

The angle of the diffracted light ( $\theta_d$ ) depends on wavelength, so diffraction by a grating, such as a muscle fiber, disperses collimated white

light into a spectrum. The diffracted light can be recollimated by a second diffraction. However, sarcomere length is variable during a contraction, so the second diffraction grating needs to have a variable spacing if the recollimation is to be maintained. An acousto-optic (A-O) device (Rosenthal, 1955; Korpel et al., 1966; Adler, 1967) is used in the present setup as the variable-spacing diffraction grating.

## Optical Components

Fig. 1 shows a simplified diagram of the optical and electronic arrangement. Light from a 75-W continuous xenon arc lamp (Xe) is collimated by a spherical lens (SL1) and passes into an A-O light beam deflector. The A-O device is a rectangular block of flint glass attached to a piezo-electric transducer, which excites traveling 30–75-MHz acoustical waves in the glass optical medium approximately normal to the direction of light propagation. The acoustic compressions and rarefactions of the glass result in small periodic changes of the refractive index that scatter light. The deflector acts as a phase diffraction grating with spacing equal to the acoustic wavelength, 50–130  $\mu$ m (Adler, 1967). The acoustic energy is absorbed at the face of the flint glass block opposite to the piezo-electric transducer.

The A-O device used in the present setup (model AOD-60A; IntraAction Corp., Bellwood, IL) was modified by the manufacturer to reduce variation of diffraction intensity with optical wavelength and diffraction angle (increasing the “Bragg-angle tolerance”). The length of the piezo-electric element in the direction of the optical propagation was reduced to  $\sim 30\%$  of the standard length resulting in generation of curved acoustic

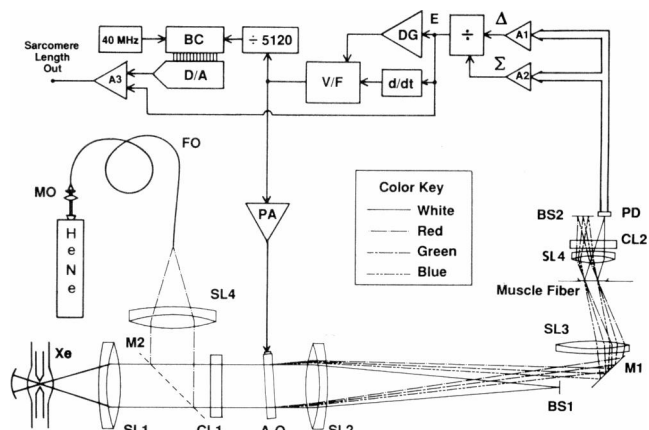


FIGURE 1 Schematic diagram of sarcomere length detector. Rays of white light are drawn as thin solid lines and rays of colored light are drawn as dashed lines as indicated in the color key. Optical components: Xe, 75-W xenon arc lamp. SL1, SL2, SL3, and SL4, achromatic spherical lenses. CL1 and CL2, singlet cylindrical lenses. A-O, acousto-optical light beam deflector. BS1 and BS2, beam stops. M1 and M2, front surface mirrors. M2 was removed for white light excitation. HeNe, helium neon laser. MO, 7.5-mm focal length, 0.4 numerical aperture microscope objective. FO, fiber optic light guide. PD, array of 16 photodiodes. Electronic components: A1, A2, and A3, summing operational amplifiers.  $\div$ , analog divider circuit. DG, direct gain feedback amplifier.  $d/dt$ , velocity feedback amplifier. V/F, voltage-to-frequency converter. PA, radio frequency power amplifier. VF and PA are part of the driver electronics (Intra-Action DE-70) for the A-O device.  $\div$  5120, binary and decade digital counter. BC, 14-bit binary counter clocked by a 40-MHz crystal oscillator; a 14-bit parallel output register holds the previous count while BC is counting. D/A, 14-bit digital-to-analog converter driven by the output register of BC. The optical-electronic feedback loop centers twice diffracted light onto PD and the Sarcomere Length Out signal is proportional to striation spacing.

wavefronts that diffract light with wide wavelength and incident angle tolerance. The wavelengths for half-maximal diffraction intensity are estimated to be 323 and 777 nm, although absorption of light by the glass optical components limits the usable spectrum to above 400 nm. The modifications to increase acceptance angle and wavelength range result in a decrease in the proportion of light diffracted from 70–80% in the standard deflector to 25–35% in the modified version.

Spherical lens SL2 focuses the light directly transmitted by the A-O deflector onto a beam stop, BS1. Light scattered into the first order diffraction beam is focused onto the muscle fiber by spherical lens SL3, positioned so that the focal planes of SL2 and SL3 coincide. SL2 and SL3 also form a real image of the A-O deflector at the muscle fiber, which is suspended in a solution trough. Light of any one color is collimated on exiting the A-O device and is also collimated at the muscle fiber. Rays from a particular point on the A-O device strike a corresponding point on the fiber regardless of color, but each color strikes the muscle fiber from a unique angle.

Cylindrical lens CL1 shapes the optical beam into a narrow line  $\sim 50 \times 3$  mm at the A-O deflector. Cylindrical lens CL2 focuses the light scattered equatorially by the muscle fiber onto a photodetector (PD). The optical interfaces between the solution bathing the muscle fiber and air above and below the trough each consist of a pair of microscope slides separated by dry air spaces to reduce moisture condensation.

SL2 and SL3 form a telescope that demagnifies the image of the A-O device at the muscle fiber by  $\sim 40$  times so that the following condition is fulfilled:

$$M = x_a/x_m = s_a/s_m, \quad (2)$$

where  $M$  is the magnification of the SL2-SL3 telescope,  $x_a$  is the position of a scattering point on the A-O device in the direction of the acoustic propagation,  $x_m$  is the position in the A-O image along the muscle fiber axis of the point corresponding to  $x_a$ ,  $s_a$  is the acoustic wavelength at the A-O deflector, and  $s_m$  is the striation spacing.

The magnification is set so that the spacing between the acoustic wavefronts projected onto the muscle fiber ( $s_a \cdot x_m/x_a$ ) is equal to the striation spacing ( $s_m$ ). If lenses SL1 and SL2 obey the sine condition (Born and Wolf, 1975), then

$$x_a \cdot \sin(\theta_{da}) = x_m \cdot \sin(\theta_{im}),$$

where  $\theta_{da}$  is the meridional angle of the beam diffracted by the A-O device at a particular wavelength, and  $\theta_{im}$  is the meridional angle of the corresponding incident ray at the muscle fiber.

Applying Eq. 1 to the first order diffraction at the A-O deflector and again at the muscle fiber,

$$\begin{aligned} x_m \cdot \sin(\theta_2) &= x_m \lambda / s_m - x_a \lambda / s_a + x_a \cdot \sin(\theta_{ia}) \\ \sin(\theta_2) &= \lambda / s_m - M \lambda / s_a + M \cdot \sin(\theta_{ia}), \end{aligned} \quad (3)$$

where  $\theta_{ia}$  is the meridional angle of the incident light at the A-O deflector, and  $\theta_2$  is the meridional angle of light diffracted once by the A-O device and then again by the muscle fiber.

If Eq. 2 is valid the first two terms on the right side of Eq. 3 cancel and the angle of the twice diffracted light ( $\theta_2$ ) does not depend on wavelength or on the position along the fiber ( $x_m$ ). Thus the resulting beam is recollimated and the chromatic dispersion of the first diffraction is reversed. The recollimated white light beam represents diffraction by the sarcomeres of light from a range of incident angles.

## Electronic Components

Eq. 3 relies on matching the image of the acoustic waves projected onto the muscle fiber with the sarcomere length (Eq. 2). Therefore when the sarcomere length ( $s_m$ ) changes, the acoustic wavelength ( $s_a$ ) must change proportionally. This tracking of the sarcomere length by the acoustic

wavelength is accomplished using a position-sensitive photodiode array in a feedback loop to control the acoustic wavelength.

The centroid position (E) of the doubly diffracted light is detected by an array of 16 photodiodes (PD in Fig. 1, Centronic Corp., Mountainside, NJ; type LD-20). PD is connected to amplifiers A1 and A2 which compute sums of the light intensity, unweighted in the case of A2, and with weights  $-15, -13, \dots, -3, -1, 1, 3, \dots, 13, 15$  in the case of A1. A divider circuit ( $\div$ , AD535; Analog Devices, Inc., Norwood, MA) computes the centroid position with respect to the center of the photodiode array as the ratio of the A1 to A2 amplifier outputs (Goldman and Simmons, 1984).

The centroid position signal (E) is connected via direct gain (DG) and velocity (d/dt) amplifiers to a voltage-to-frequency (V/F) convertor and a radio frequency (30–75 MHz) power amplifier (PA), which drives the piezo-electric ultrasonic transducer of the A-O deflector. The photodiodes are placed so that E is nulled when the acoustic frequency is adjusted as described below to match the sarcomere length. The feedback maintains a constant angular position,  $\theta_2$ , of the doubly diffracted light by centering the doubly diffracted light on the photodetector. E is then the error signal for the optical feedback loop. When the feedback loop is balanced, the acoustic wavelength (and also the time interval between acoustic wavefronts) is directly proportional to sarcomere length (Eq. 2) and the conditions for reversal of chromatic dispersion and recollimation of the doubly diffracted light are simultaneously fulfilled.

The 30–75-MHz ultrasonic driving signal for the A-O piezo-electric transducer is amplitude modulated with a 20-kHz square wave, and the photodetector circuitry incorporates two sample-and-hold circuits triggered on the on and off phases of the modulating signal. The difference between the outputs of the two sample-and-hold circuits is used as the demodulated position signal. This modulation–demodulation eliminates stray light components. An integrator in the direct gain amplifier increases the low frequency loop gain so that the error at zero frequency is essentially null (Goldman and Simmons, 1984). The electro-optical feedback loop settles (10–90%) in 0.3 ms after a perturbation.

The sarcomere length is directly proportional to the time interval between acoustic wavefronts, which is the reciprocal of the A-O driving frequency. A 14-bit binary counter circuit (BC) performs the required reciprocal conversion. This register counts pulses from a 40-MHz crystal oscillator for an interval corresponding to 5,120 cycles of the 30–75-MHz ultrasonic signal. A binary output register is updated at 6–15 kHz and its value converted by a digital-to-analog (D/A) convertor to a sarcomere length signal with resolution equivalent to 0.06 nm per half sarcomere.

The bandwidth of the sarcomere length signal is enhanced by feedforward compensation (Goldman and Simmons, 1984) in which a linear combination of the error signal (E) and the D/A convertor output is formed by amplifier A3. In the output signal, the highest frequency components (3–20 kHz) are derived directly from the photodetector circuitry and the signal components below 3 kHz are derived from the digitally calculated period of the ultrasonic signal. The output signal is updated every 50  $\mu$ s and the overall usable bandwidth of the sarcomere-length signal is  $\sim 10$  kHz. Noise is equivalent to  $\sim 0.1$  nm per half sarcomere.

## Adjustment and Calibration

Fig. 2A shows the diffraction pattern obtained from a relaxed frog skinned muscle fiber. The spectrum (labeled  $I_{da}$ ) was diffracted once by the A-O device and then transmitted by the muscle fiber. The band of white light ( $I_0$ ) was diffracted again by the muscle fiber and represents diffraction of light from a range of incident angles.

To initially set the acoustic frequency so that the image of the acoustic wavefronts at the muscle fiber matches the sarcomere length (Eq. 2), the beam stop (BS1 in Fig. 1) and the muscle fiber are moved out of the optical path, producing the pattern in B.  $I_0$  is light transmitted through the whole optical system without scattering. A mask that splits the pattern across the meridian is then placed in the position of BS1 producing the pattern in C. On one side of the meridian the mask blocks

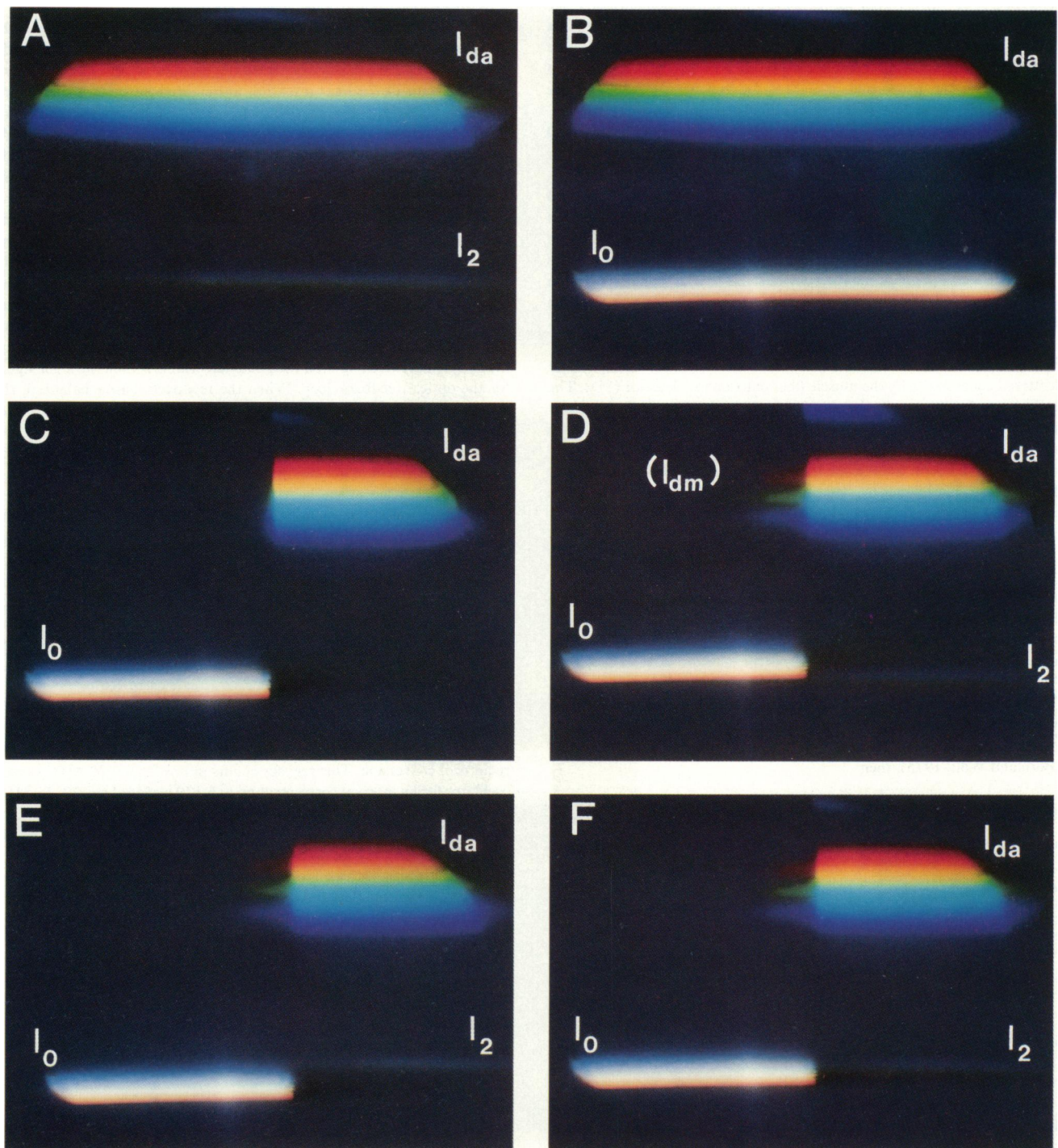


FIGURE 2 Diffraction spectra and adjustment procedure for the sarcomere length monitor. The spectra were recorded at the position of the photodiodes (PD) and beam stop (BS2) in Fig. 1 with cylindrical lens CL2 and spherical lens SL4 removed. (A) Spectrum with muscle fiber in place.  $I_{da}$  is light diffracted by the A-O deflector and transmitted through the muscle fiber.  $I_2$  is light diffracted again by the cross-striations. (B) Spectrum of the A-O device alone. Beam Stop (BS1) was removed and the muscle fiber was not in place.  $I_0$  is light transmitted through the entire optical system without diffraction. (C) Spectrum as in B but with a mask placed at the position of BS1 to transmit half of  $I_0$  and half of  $I_{da}$ . (D) Spectrum as in C but with the muscle fibers in place; note that  $I_2$  is not aligned with  $I_0$ . (E) Spectrum as in D but with the A-O acoustic wavelength reduced by 18%. The misalignment between  $I_0$  and  $I_2$  is reversed. (F) Spectrum as in D and E but with the acoustic wavelength set to align  $I_0$  and  $I_2$ . After adjusting the acoustic wavelength as in F, the split mask was replaced by BS1 to record A.

light directly transmitted by the A-O device but allows the first order diffraction beam ( $I_{da}$ ) through. On the other side of the meridian, light diffracted by the A-O device is blocked, but directly transmitted light ( $I_0$ ) is allowed through. When the muscle is moved into place ( $D$ ), two more diffraction bands appear:  $I_{dm}$ , light transmitted directly by the A-O device and diffracted once by the muscle fiber, and  $I_2$ , doubly diffracted light.  $I_{dm}$  is faint compared with the other bands and may not be appreciable in the final printed plate. The acoustic wavelength in  $D$  was greater than the value satisfying Eq. 2 by  $\sim 9\%$ . This causes misalignment across the meridian between  $I_2$  and  $I_0$ . Decreasing the acoustic wavelength by 18% results in the diffraction pattern of Fig. 2 *E*. The misalignment across the meridian is reversed. The condition of correct matching between the directly transmitted light ( $I_0$ ) and the twice diffracted light ( $I_2$ ) is shown in *F*. The same setting for the acoustic frequency also aligns the two singly diffracted spectra,  $I_{dm}$  and  $I_{da}$ .

The position of mirror M1 (Fig. 1) is set so that the incident angle of green light near the center of the visible spectrum ( $\lambda \approx 550$  nm) equals the angle of the doubly diffracted white light, and transverse striations are at the Bragg angle for that wavelength. When the sarcomere length is  $2.25 \mu\text{m}$ , the incident angles for light at 400, 550, and 700 nm (wavelengths in air) are  $2.3^\circ$ ,  $5.1^\circ$ , and  $7.9^\circ$  (angles within the fiber assuming its index of refraction is 1.375).

After these adjustments, the split mask is removed and beam stop BS1 is replaced (Fig. 2 *A*). The photodiode array is installed in the meridian of the diffraction plane and it is centered on the diffraction peak. With the optical feedback loop in operation the instrument then provides a signal linearly related to sarcomere length. Glass-mounted diffraction grating replicas are positioned in place of the fiber to calibrate the scale and offset of the sarcomere length signal.

### Laser Illumination

To compare the white light method with laser diffraction, mirror M2 (Fig. 1) is inserted into the optical path to select the light from a 5-mW helium neon (HeNe) laser (model 120; Spectra-Physics Inc., Mountain View, CA). The laser beam is expanded to the diameter appropriate for the acousto-optical device (50 mm) by a  $10\times$  microscope objective (MO) and spherical lens SL4. When the sarcomere length is  $2.25 \mu\text{m}$ , the incident angle of the laser light within the fiber is  $6.6^\circ$ .

For some types of experiment (Fig. 5), the coherence of the laser light is reduced by inserting a 1-m length of  $100\text{-}\mu\text{m}$  diam fiber optic light guide (FO in Fig. 1; Newport Research Corp., Fountain Valley, CA; type

F-MLD-10) in the laser beam expander. The fiber optic light guide is moved or vibrated to alter the path length for various rays within the light guide and thus reduce the coherence (Ellis, 1979). For most experiments with laser light (Figs. 4 and 6) the fiber optic was not used and MO and SL4 were positioned with coinciding focal planes.

## RESULTS

### Tests of the Instrument

To determine the reproducibility of the correct acoustic frequency obtained by matching the position of the doubly diffracted light with the light transmitted directly through the system, the adjustment procedure of Fig. 2 was repeated 20 times for several fibers. The standard deviation of the matching frequency obtained as in Fig. 2 *F* was 0.6–0.7%. This corresponds to an uncertainty of  $\pm 15$  nm per sarcomere in the absolute signal.

The calibration of the system for small changes in sarcomere length was checked as described for the previously reported laser diffraction system (Goldman and Simmons, 1984). A small stretch was applied to fibers and the output of the diffraction instrument was compared with the signal expected from microscopic measurements. Fig. 3 *A* shows the magnitude of axial movements of a fiber during a series of  $20\text{-}\mu\text{m}$  stretches and releases applied in relaxing solution (*circles*) and in rigor (*squares*). The axial movements are plotted vs. the position along the fiber. If the compliance is distributed uniformly along the fiber, the data should fall along a straight line as in the relaxed case. In the rigor contraction, a substantial series compliance is apparent in the larger proportion of movement occurring at the ends. Thus, for a given length step applied to the fiber, the predicted change in sarcomere length is less in rigor than in relaxing solution.

Using the diffraction instrument with white light,

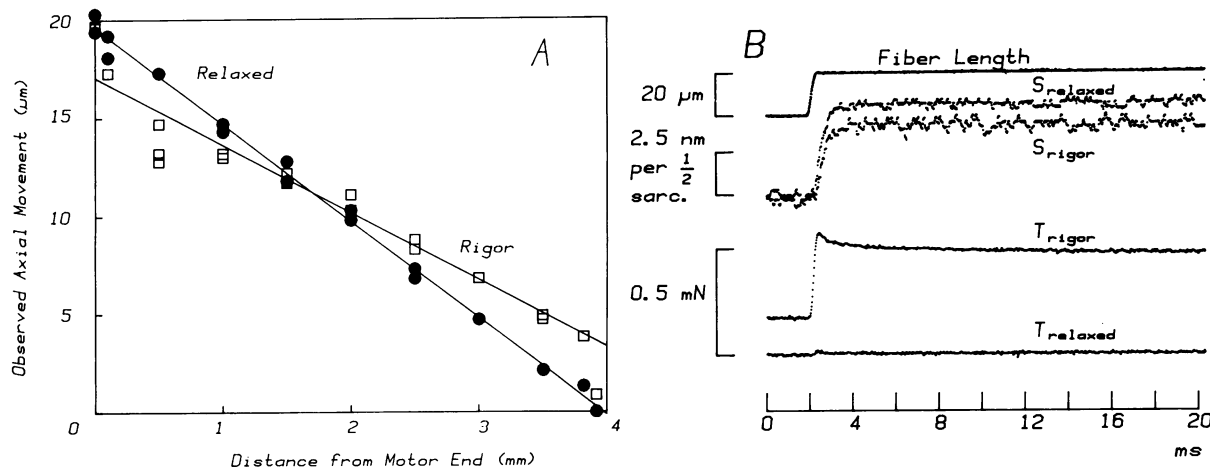


FIGURE 3 Comparison of microscopic estimate of sarcomere length change with output from diffraction device. (*A*) Movement observed through a compound microscope when the fiber was repeatedly stretched and released by  $20 \mu\text{m}$  in relaxing solution ( $\bullet$ ) and in rigor ( $\square$ ). A significant end compliance is present in rigor. (*B*) Recorded fiber length change (*top trace*), sarcomere length change (*middle traces*), and tension (*bottom traces*). Note that the sarcomere length change is less in rigor. Fiber dimensions,  $3.99 \text{ mm} \times 25.9 \cdot 10^3 \mu\text{m}^2$ ; sarcomere length,  $2.04 \mu\text{m}$ .  $T = 1.4^\circ\text{C}$ .

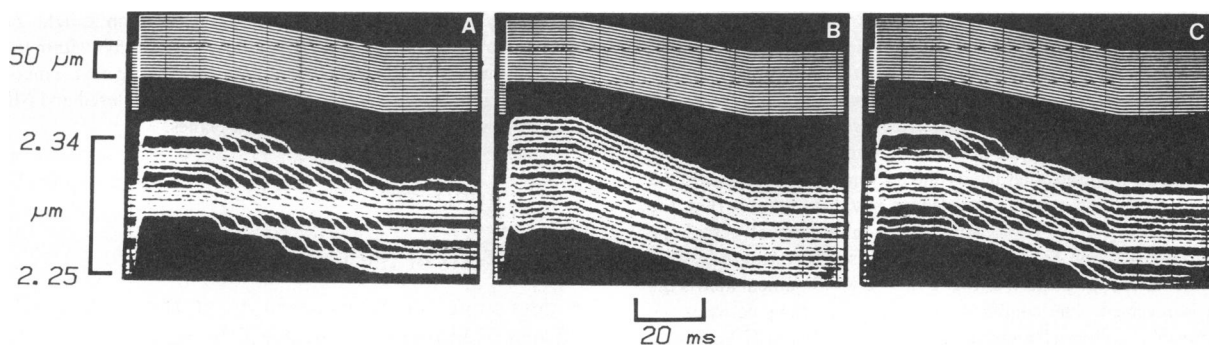


FIGURE 4 Length signals during repeated passive stretch and ramp releases with a fiber in relaxing solution. Upper traces are overall length change. Lower traces are the output from the sarcomere length monitor. Each stretch–release cycle was initiated from a different starting length. In *A* and *C* the xenon arc lamp was replaced with a HeNe laser source by placement of mirror M2 (Fig. 1) in the optical path. In *B* mirror M2 was removed enabling the Xe arc lamp illumination. Sarcomere length,  $2.25 \mu\text{m}$ .

recordings of the sarcomere length from a central 1.8-mm illuminated segment of the fiber show that the amplitude of the step is less in rigor than in relaxing solution (Fig. 3 *B*). In a series of 10 such measurements, the sarcomere length output of the A-O diffraction setup matched the results of the microscopic measurement to within  $\pm 5\%$  or  $\pm 0.5 \text{ nm}$  per half sarcomere for a step of 10 nm per half sarcomere.

#### Steps and Pauses in Relaxed Fibers

Fig. 4 shows sarcomere length signals (lower set of traces) and motor movement (upper set of traces) recorded during repeated stretches and ramp releases of a frog skinned fiber in relaxing solution. Each trace started at a slightly different length. In this experiment, the source of illumination was switched between the xenon arc lamp and coherent light from a HeNe laser (see Methods). The optical path was otherwise the same. The overall length of the muscle fiber decreased smoothly but when the source of illumination was the laser, the decrease in the sarcomere length signal was not steady. Steps and pauses are apparent in the recordings with laser light (Fig. 4 *A*). Comparison of the traces starting at different lengths shows that the steps were highly reproducible in successive traces and occurred at certain sarcomere lengths rather than at particular times in the sweep. The sarcomere length trace typically decreased irregularly during steady passive shortening if laser illumination was used, but in most fibers, the alterations in the slope of the traces were less abrupt than in Fig. 4.

Replacing the laser source with white light from the xenon arc lamp eliminated steps and pauses in passively shortening fibers (Fig. 4 *B*), suggesting that the nonsteady decrease of the sarcomere length signal is related to the type of illumination. A control run with laser illumination (*C*) shows reappearance of the steps and pauses.

Two factors might contribute to the reduction or elimination of steps and pauses with white light as shown in Fig. 4: (a) the white light is less coherent than laser light, and (b) the various colors enter the fiber at different angles and

thereby select sarcomere domains with striations having a range of Bragg angles. To distinguish between these hypotheses, the coherence of the laser light was reduced using a method that causes little change in the illumination angle. The HeNe laser light was passed through a fiber-optic light guide as described in the Methods section. Bending of the fiber-optic strand changed the optical path length difference between rays within the fiber-optic medium and therefore altered their optical phase relationship.

Fig. 5 shows muscle length (*top trace*) and sarcomere length (*lower traces*) during length steps and shortening ramps in a relaxed fiber. A section of the fiber was located, which showed pauses in the sarcomere length signal (*arrows*). A loop of the fiber optic light guide was moved through an angle of  $\sim 30^\circ$ , which had the effect of twisting

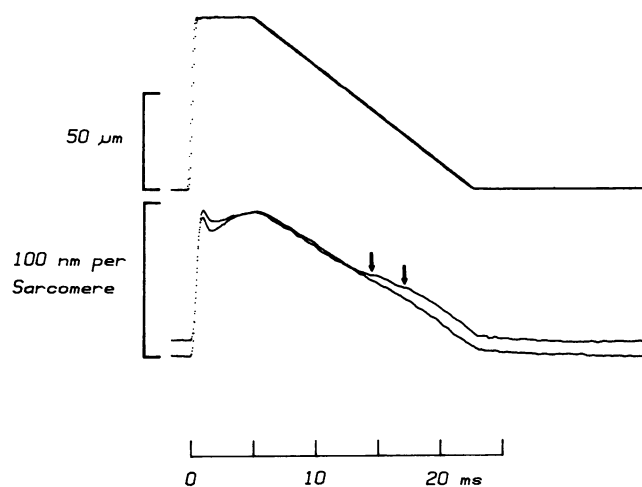


FIGURE 5 Length signals during passive stretch and ramp release with laser illumination. Upper traces are superimposed overall length changes. Lower traces are output of the sarcomere length monitor. Arrows point to pauses in the output signal during the steady shortening. The fiber-optic light guide (FO in Fig. 1) was moved to alter the coherence of the laser light and the lower sarcomere length trace was recorded. The pauses were eliminated. Sarcomere length,  $2.25 \mu\text{m}$ .  $T = 3.1^\circ\text{C}$ .

the light guide by the same amount. This markedly altered fringes in the beam indicative of wavefront distortion and thus had the effect of altering the relative optical phase across the beam. The muscle fiber length change was repeated and the pauses were eliminated in the resulting sarcomere length trace (*lowest trace*).

A series of eight fibers were tested as in Fig. 5 for elimination of steps and pauses by shifting the position of the fiber optic. Six of them showed clear steps and pauses over some interval of passive shortening. The pauses were reproducible during repeated length changes. However, movement of the fiber optic to another static position eliminated or substantially reduced the irregularities on the sarcomere length trace. In a few examples at short sarcomere lengths, the muscle fiber went slack briefly during the shortening and irregular deflections of the sarcomere length trace were not modified by movements of the fiber optic. Since these cases always occurred near to a slackening condition, they were probably caused by a lateral movement of the fiber.

The results suggest that at sarcomere lengths above slack length the steps and pauses observed were the result of the high degree of coherence of laser light. Altering the coherence modified the shape of the irregularities and usually eliminated them.

### Active Contractions

The striation pattern of skinned fibers generally deteriorates during steady active contractions. Brenner (1983) described a method to improve the uniformity of glycerol-extracted fibers from rabbit psoas muscle during active contractions. The fibers were "cycled" repeatedly through

a period of rapid isotonic shortening, a rapid stretch, and finally an isometric interval at the extended length.

In the present work the cycling method was applied to frog skinned fibers. Fig. 6 shows records of active tension (*bottom traces*), overall length (*middle*), and sarcomere length (*top*) of a frog muscle fiber during the cycling procedure at pCa ( $-\log[\text{Ca}^{2+}]/M$ ) 5.9. The active tension development was  $\sim 50\%$  of fully activated tension. As expected, the motor and sarcomere length signals (using white light) have similar shapes during isotonic shortening. At submaximal activation the velocity of shortening decreases gradually during the isotonic phase as described previously (Brenner, 1980; Ferenczi et al., 1984; Julian et al., 1986). When an abrupt stretch is applied during isotonic shortening, an initial tension transient is followed by tension recovery to the isometric level during the next few seconds. During the tension recovery the sarcomere length decreases slightly, indicating stretch of the end compliance. The cycling method improved the uniformity of cross-striations with frog fibers enough to allow contractions to be completed at  $\text{Ca}^{2+}$  concentrations giving up to 60–80% of maximal active tension. However, saturating  $\text{Ca}^{2+}$  concentrations still resulted in disorganization of the sarcomere structure and loss of the diffraction pattern.

Fig. 7 shows a comparison of the sarcomere length signals with white light and laser light during active isotonic contractions at 5 mM MgATP and pCa 5.9. The time of the oscilloscope trigger was varied to separate the traces from successive cycles. Pauses and periods rapid of shortening are apparent on the traces recorded with laser illumination (Fig. 7 *A*). As in relaxed fibers, the shortening was smooth when white light illumination was used (*B*), suggesting that the steps and pauses result from laser

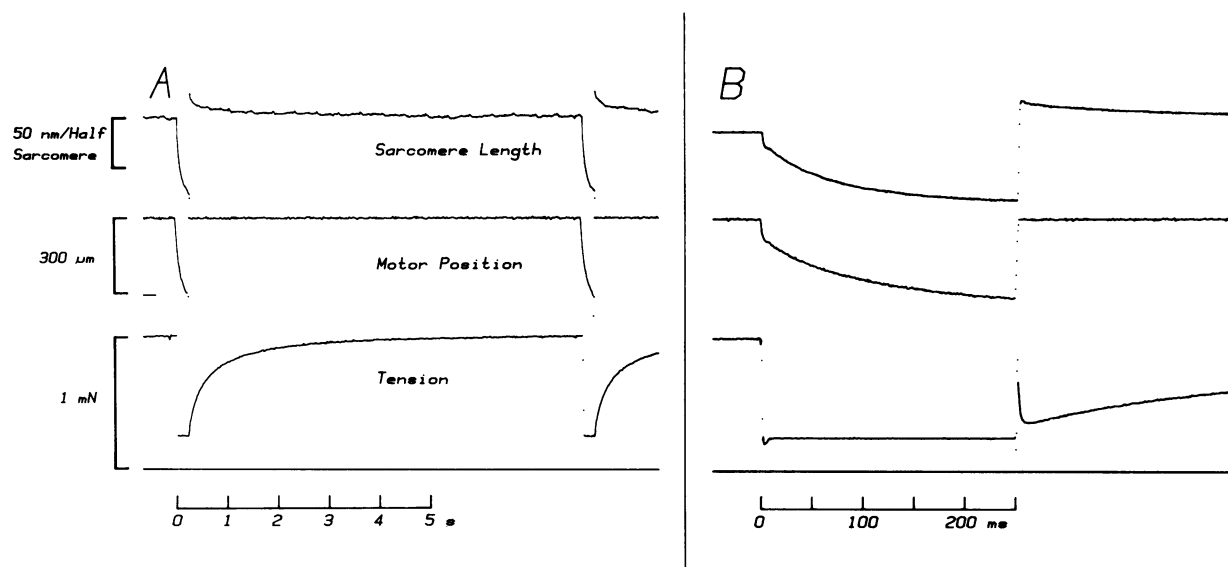


FIGURE 6 Cycling procedure of Brenner (1983) applied to a frog skinned muscle fiber. *A* and *B* are equivalent recordings at two sweep speeds. *Upper traces*, output from sarcomere length monitor. *Middle traces*, overall length change. *Lower traces*, tension. *Lowest flat traces*, tension baseline. The fiber was repeatedly allowed to shorten isotonicly and was then rapidly stretched to the original length.  $[\text{Ca}^{2+}] = 1.14 \mu\text{M}$ . Sarcomere length,  $2.26 \mu\text{m}$  during the isometric phase.

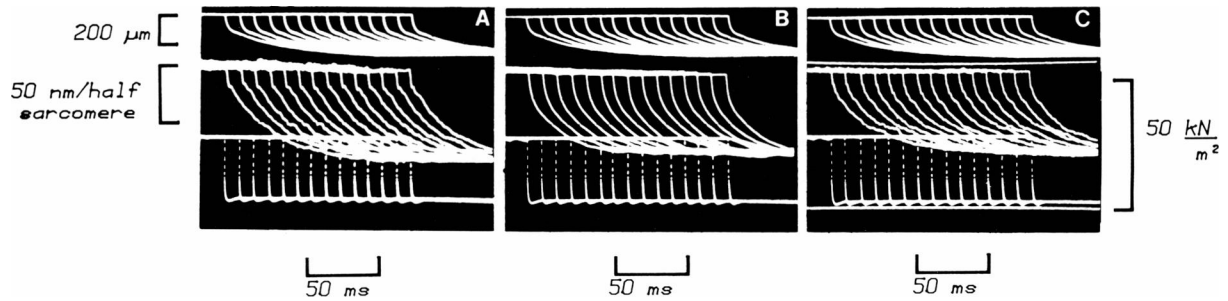


FIGURE 7 Length recordings repeated during active isotonic contractions. (A and C) Laser illumination (B) Xe arc lamp illumination. Upper traces, overall length change. Middle traces, output from sarcomere length monitor. Lower traces, tension. The lowest flat trace in C is the tension baseline.  $[Ca^{2+}] = 1.14 \mu M$ . Fiber dimensions,  $2.65 \text{ mm} \times 22.6 \cdot 10^3 \mu m^2$ ; sarcomere length,  $2.55 \mu m$  during the isometric phase.  $T = 4.6^\circ C$ .

illumination. A control run with laser illumination (C) shows reappearance of the steps and pauses.

### Force–Velocity Curve

During the cycling procedure, the force–velocity relationship was determined by interposing isotonic periods at various loads. Fig. 8 A shows the recordings using the white light method from such a series of isotonic contractions at pCa 6.0 leading to  $\sim 30\%$  activation. As noted above, shortening velocity decreases during the isotonic phase of the contraction, so velocities were measured at the time corresponding to stabilization of the tension trace, 5–10 ms after the load step. The velocity increased markedly as the load was reduced to very low values. At loads below  $\sim 5\%$  of the isometric tension, the recorded sarcomere shortening velocities were typically  $3\text{--}5 \mu m/s$  per half sarcomere, which are higher than usually reported for intact fibers. The recorded velocities were highly sensitive to small changes of the value of the load near zero load.

The velocities recorded early in the isotonic phase are plotted vs. relative tension in Fig. 8 B. The best fit hyperbolic curve of the form  $(P + a) \cdot (V + b) = c$  (solid line) does not fit the data very well and falls below the data points at relative tensions 0.2–0.6. If a hyperbolic curve is fitted to the data excluding the two highest velocity points, a better fit is achieved (dashed curve) but the data points at relative tension  $< 0.05$  are above the curve. This deviation from a hyperbolic force–velocity curve at low loads confirms previous reports on frog skinned fibers (Goldman, 1983; Rome et al., 1985; Julian et al., 1986). There is less deviation between a hyperbolic curve and the force–velocity data in intact fibers (Edman, 1979; Julian et al., 1986).

Another difference between skinned and intact frog fibers is that the immediate force–extension curve of skinned fibers is less steep (Goldman and Simmons, 1986). Shrinkage of the swollen skinned fiber filament lattice toward the normal dimension with osmotic agents partly restores the stiffness (Goldman and Simmons, 1986), so it

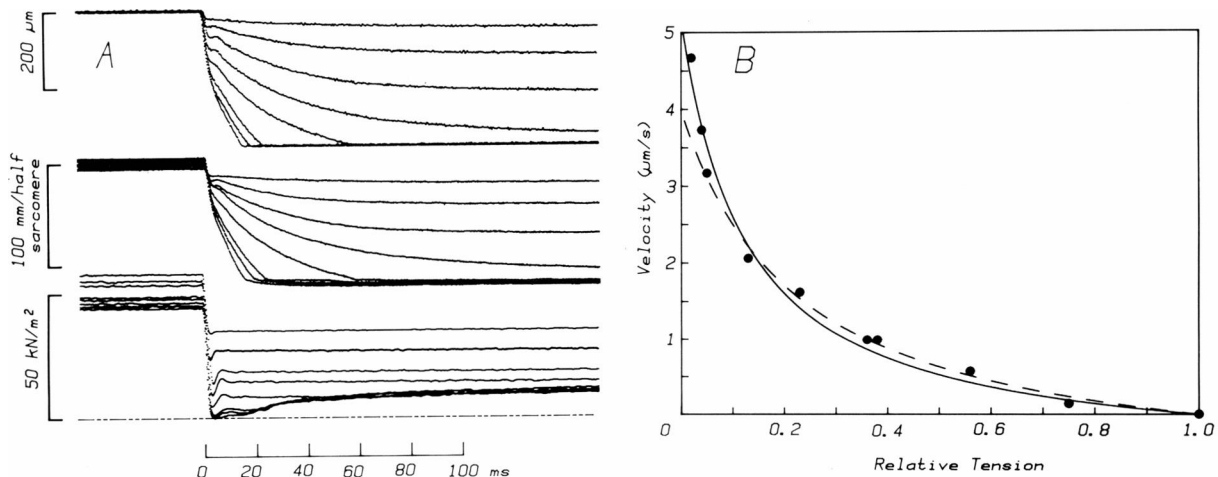


FIGURE 8 Recording of the force–velocity curve. (Left) The cycling procedure of Fig. 6 was modified by altering the isotonic force level to obtain shortening velocities for various loads. Traces are as in Fig. 7. (Right) Velocities recorded 10 ms after the load step are plotted versus the isotonic tension relative to isometric tension. The solid curve is the best fit rectangular hyperbola to the data. The dashed curve is the best fit to the data excluding the two highest velocity points.  $[Ca^{2+}] = 0.98 \mu M$ . Fiber dimensions,  $4.12 \text{ mm} \times 25.3 \cdot 10^3 \mu m^2$ ; sarcomere length,  $2.60 \mu m$  during the isometric phase.  $T = 3.0^\circ C$ .

was of interest in the present study to test the effect of osmotic shrinkage on the force-velocity curve. The "cycling" procedure was used to obtain repeated isotonic contractions during partial  $\text{Ca}^{2+}$  activation.

Fig. 9 shows the effect of osmotic agents PVP-40 (60 g/liter) and dextran T-500 (50 g/liter) on the velocities of isotonic sarcomere shortening. The polymers reduce the velocity at low loads. The  $V_{\max}$  values estimated by extrapolation of the hyperbola fitted to the force velocity data were  $4.43 \mu\text{m/s}$  per half sarcomere ( $\pm 0.80$  SEM,  $n = 15$ ) in the absence of added polymer,  $2.61 \mu\text{m/s}$  ( $\pm 0.25$ , SEM,  $n = 8$ ) at 60 g/liter PVP and  $2.54 \mu\text{m/s}$  ( $n = 2$ ) at 50 g/liter dextran.

The slack test (Edman, 1979) was also used to measure  $V_{\max}$  at full activation. Skinned frog muscle fibers shortened at  $5.49 \mu\text{m/s}$  ( $\pm 1.29$  SEM,  $n = 4$ ) per half sarcomere at  $T = 5^\circ\text{C}$  in the absence of osmotically active polymers and at  $2.87 \mu\text{m/s}$  ( $n = 2$ ) in the presence of 60 g/liter PVP-40. The reduction of shortening velocity in isotonic contractions or in the slack test was fully reversible on removal of the polymer.

## DISCUSSION

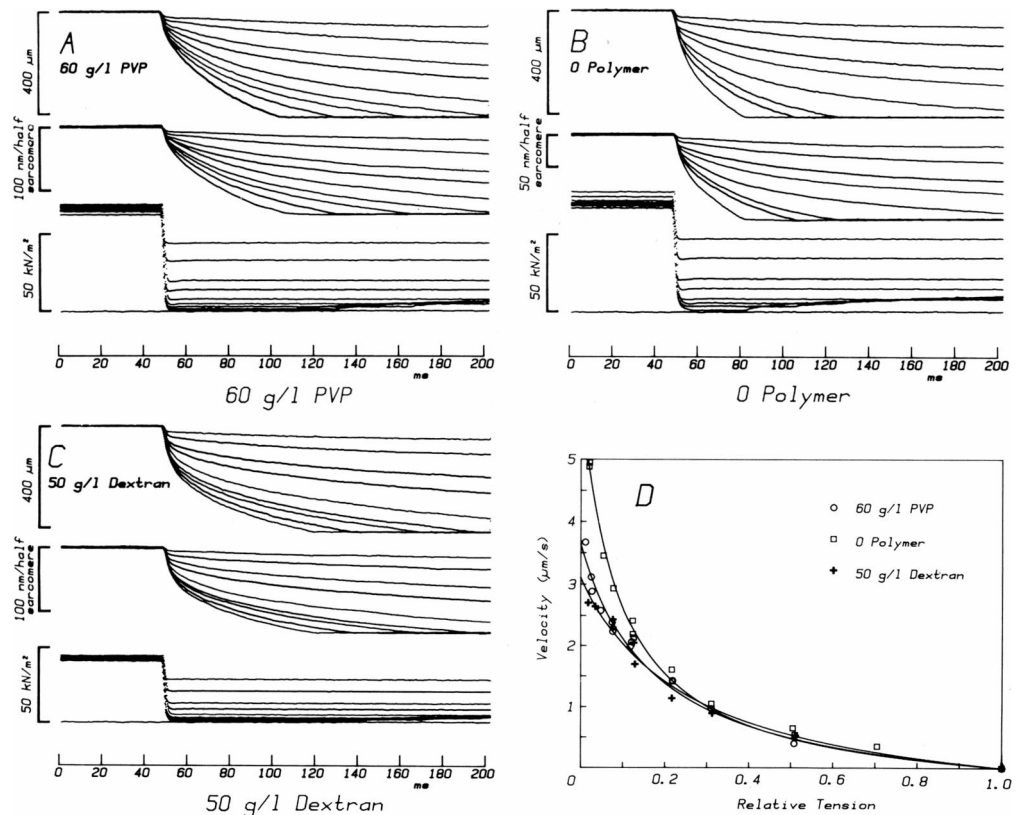
### Steps and Pauses During Steady Shortening

The method for monitoring striation spacing presented here is an extension of the laser diffraction system described by Goldman and Simmons (1984). In both

setups, when collimated and coherent laser light was used to illuminate the muscles for diffraction measurements, the signal deviated from the average striation spacing. Reducing the coherence and collecting the signal from light representing a range of incident angles reduced or eliminated these artifacts. In frog skinned muscle fibers, steps and pauses in the striation spacing signal during active and passive shortening were also eliminated by these maneuvers. The two simplest explanations for this behavior are that the steps and pauses are caused by (a) Bragg-angle effects (Rüdel and Zite-Ferenczy, 1979, 1980) or (b) cross-interference between light scattered from different sarcomere domains (Sundell et al., 1986; Brenner, 1985).

With an object that is thick compared with the light wavelength, rays scattered from different depths will interfere constructively at the diffraction plane only if the illumination angle is near the Bragg-angle (half the diffraction angle; Bragg, 1933) with respect to the lattice planes (the cross-striations in the case of muscle fibers). The Bragg-angle changes as the fiber shortens, so cross-striations will not generally be oriented accurately at the Bragg-angle throughout the fiber and throughout a contraction. If this mechanism selects sarcomere regions that differ in striation spacing by a few percent, then irregularities like steps and pauses would be expected during steady shortening. The striation spacing signal from light representing a range of incident angles would include contributions from a more representative sample of the sarcomeres in the muscle fiber, so the observed elimination of steps and

FIGURE 9 Force-velocity curves recorded when the lateral spacing of the filament lattice was altered. In A-C the recording conditions were similar to those of Fig. 8 except 60 g/liter PVP-40 was present in A and 50 g/liter dextran T-500 was present in C. Velocities measured 10 ms after the load step are plotted in D versus isotonic tension relative to isometric tension in each solution. The polymers reduce shortening velocity mainly at low loads.  $[\text{Ca}^{2+}] = 0.98 \mu\text{M}$ . Fiber dimensions,  $3.18 \text{ mm} \times 31.8 \cdot 10^3 \mu\text{m}^2$ ; sarcomere length,  $2.32 \mu\text{m}$  during the isometric phase.  $T = 3.5^\circ\text{C}$ .



pauses with white light diffraction is expected on the Bragg-angle hypothesis. With the present setup, the angle of the incident light varies  $\sim 5.6^\circ$  between wavelengths of 400 and 700 nm so cross-striations with at least a  $2.8^\circ$  range of orientations (centered on the transverse orientation) are represented in the striation spacing signal.

Another possible reason that regions of striations may fail to make appropriate contributions to the diffraction pattern is destructive interference between domains of sarcomeres that are relatively uniform in striation spacing and inclination (Sundell et al., 1986). Large domains lead to bright regions in the diffraction pattern, but arrival of diffracted light from two domains at the same area of the diffraction pattern can lead to destructive interference (Sundell et al., 1986) and even the appearance of several interference fringes (Brenner, 1985). The relative phase between two such diffracted beams and thus the cross-interference effect alters during fiber shortening, so this mechanism may select which regions of the fiber dominate the diffraction spectrum. Again the steps and pauses during steady shortening may be explained by changes in the domains making the most significant contributions to the diffraction pattern. Changing the angle of the incident light alters the phase difference between cross-interfering beams, so if the incident angle is varied, the cross-interference will oscillate between the constructive and destructive conditions. Cross interference effects will cancel in the average striation spacing signal taken from a range of incident angles.

The cross-interference mechanism requires that the coherence length of the light be greater than the physical separation of the interfering domains, a condition fulfilled by light from a typical commercial HeNe laser. Altering the wavefront of the laser light without greatly changing the incident angle either reduced the prominence or eliminated steps and pauses (Fig. 5), suggesting that the cross-interference mechanism contributes to the appearance of these artifacts. However, the Bragg-angle mechanism and other possible mechanisms (Altringham et al., 1984) probably also contribute to these artifacts.

The results show clearly that laser diffraction in its usual form does not give reliable striation spacing signals representing the whole volume illuminated by the laser beam. Therefore, the inference made in previous papers that the steps and pauses imply synchronization of sarcomeres over the entire illuminated region (Pollack et al., 1977; Delay et al., 1981; Pollack, 1986) is not correct. If the sarcomeres were synchronized, then signals from white light diffraction would also show steps and pauses. This is contrary to the results of Figs. 4–6 and those of Goldman and Simmons (1984), showing that the optical configuration (particularly the coherence and incident angle) markedly influences the steps and pauses.

The possibility that motions within small regions of sarcomeres occur in synchrony is not eliminated by the present results, since the region illuminated (1.8-mm

length of fiber) is larger than is customary in the experiments of Pollack and co-workers. The results do not bear on other methods of detecting steps and pauses (Brozovich and Pollack, 1983; Granzier and Pollack, 1985), but laser light diffraction (and similarly image plane analysis using laser light illumination; Delay et al., 1981) should not be considered corroborative to those methods.

### White Light Diffraction

The main advantage of using white light for muscle fiber diffraction is that the Bragg-angle depends on wavelength, so a range of striation tilts is automatically accommodated by various wavelengths in the illuminating beam. A disadvantage is that the diffraction angle also depends on wavelength (chromatic dispersion). The spectrum produced by diffraction of collimated white light would spread over  $\sim 5^\circ$  and the diffraction angle would be difficult to measure precisely. This problem has been eliminated in the present setup by a preliminary diffraction in a A-O device and an optical arrangement that causes a second diffraction by the muscle fiber to reverse the chromatic dispersion and to recollimate the light. A null-detecting servo maintains this condition during contractions. The striation spacing is conveniently computed on line.

Another problem is more difficult to get around. The intensity of the twice-diffracted light is low and this determines the effective bandwidth and noise level. When skinned fibers are activated by rapid changes in  $\text{Ca}^{2+}$  concentration, the disorder of the striations increases and the intensity of diffracted light decreases. The system was not useful at full  $\text{Ca}^{2+}$  activation for this reason, but using the cycling procedure of Brenner (1983), activation levels of 60–80% were achieved in many fibers with diffraction patterns intense and sharp enough to monitor striation spacing accurately.

### Skinned Fiber Force–Velocity Curve

An example of the use of the diffraction instrument is to examine the force–velocity curve in skinned muscle fibers. Deviations between the overall length and the striation spacing signal in Figs. 6 and 7 confirm that there is substantial end compliance in these skinned muscle fibers as reported before (Goldman and Simmons, 1984; Ferenczi et al., 1984). Thus sarcomere length detection or other means to correct for end compliance is necessary.

The force–velocity curves obtained from frog skinned muscle fibers are very steep in the low force region, and velocity increases sharply as force is reduced to near zero (Fig. 8). This result confirms the findings of Rome et al. (1985) and Julian et al. (1986) who found a deviation from a hyperbolic curve of the force–velocity relation in skinned fibers shortening at low loads. Shrinkage of the swollen filament lattice toward its normal value reduced  $V_{\max}$  and the steep increase of velocities at very low loads (Fig. 9). Gulati and Babu (1984) found that osmotic shrinkage also

reduces  $V_{\max}$  of intact fibers. The present results suggest an explanation, related to the influence of osmotic compression on the cross-bridge force–extension curve.

The filament lattice of a muscle fiber expands when the membrane is removed (Matsubara and Elliott, 1972; Matsubara et al., 1984). Goldman and Simmons (1986) found that skinned muscle fibers are less stiff than intact muscle fibers even when the end compliance is effectively removed by a feedback sarcomere length clamp. The immediate force–extension curve of skinned fibers has a tail of positive tension for releases up to at least 12 nm per half sarcomere. For comparison, the force–extension curve of a skinned fiber restored to its normal lattice spacing by osmotic compression or of an intact fiber is more linear and intersects the abscissa at an acute angle for release of 4–6 nm per half sarcomere. The intercept implies that cross-bridges can exert a negative force when the strain is negative (Ford et al., 1977). If this were not the case the force–extension curve would approach the abscissa asymptotically as in swollen skinned fibers. These points led to the hypothesis that in skinned fibers the cross-bridges buckle under compressive load (Goldman and Simmons, 1986).

What effect would this hypothetical buckling have on the force–velocity curve? The model of A. F. Huxley (1957) postulates that the maximum shortening velocity of an intact muscle fiber is set by a balance between cross-bridges exerting positive force and cross-bridges causing drag before detaching in the region of negative force. If cross-bridges in skinned fibers are less able to exert such negative forces, then this balance of forces would occur at higher velocities.

This idea can be quantitated within the framework of the Huxley (1957) model by defining two values for cross-bridge stiffness:  $k_1$  for positive strain, and  $k_2$  for negative strain. The equation for force as a function of velocity becomes

$$P = P_0 \left\{ 1 - \frac{V}{\phi} (1 - e^{-\phi/V}) \cdot \left[ 1 + \frac{1}{2} \frac{k_2 (f_1 + g_1)^2 V}{k_1 (g_2)^2 \phi} \right] \right\},$$

where  $P$  is force,  $V$  is velocity,  $P_0$  is isometric force,  $f_1$  is a parameter defining the rate constant for attachment at positive strain,  $g_1$  is a parameter defining the rate constant for detachment at positive strain,  $g_2$  is a rate constant for detachment at negative strain,  $\phi$  is  $(f_1 + g_1) \cdot h/s$ ,  $h$  is the cross-bridge attachment range,  $s$  is the sarcomere length,  $k_1$  is the cross-bridge stiffness at positive strain, and  $k_2$  is the cross-bridge stiffness at negative strain.

This equation is plotted in Fig. 10 for several values of relative stiffness,  $k_2/k_1$ . As the stiffness for negative strain ( $k_2$ ) is decreased, the calculated velocity at low loads increases. This behavior can be compared with the force–velocity curves of the skinned fiber as it is swollen on skinning or by removing polymer (Fig. 9). The increase in velocity is most prominent at low loads as expected if cross-bridges tend to buckle in swollen fibers and therefore cannot support a compressive load.

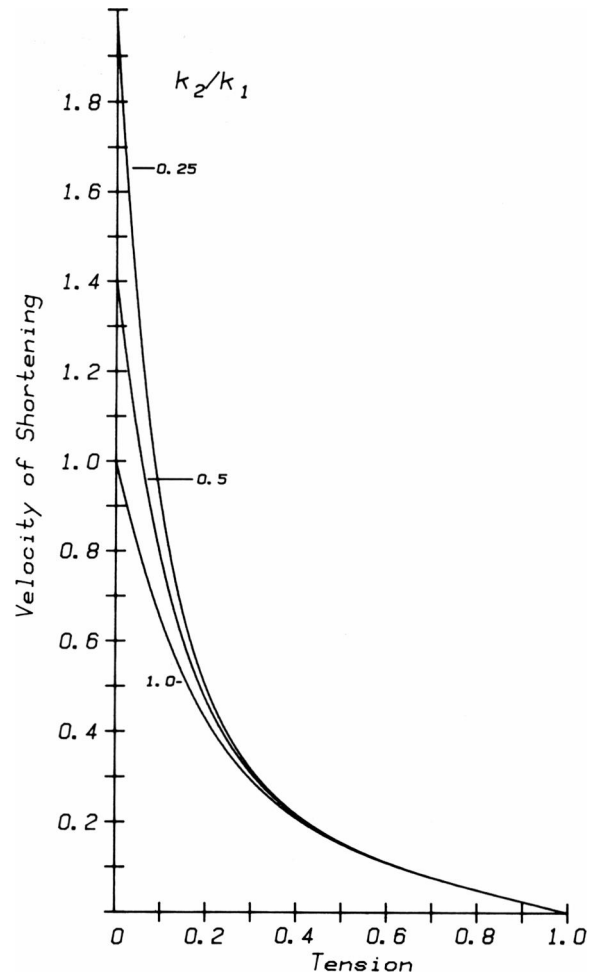


FIGURE 10 Theoretical force–velocity curves according to the model of Huxley (1957) modified to incorporate reduced cross-bridge stiffness at negative strain.  $k_2/k_1$  is the ratio of cross-bridge stiffness in the region of negative strain ( $k_2$ ) relative to that at positive strain ( $k_1$ ). Force and velocity are plotted relative to  $P_0$  and  $V_{\max}$  at  $k_2/k_1 = 1$ . As  $k_2$  is reduced, the predicted velocity at low loads increases.

Other explanations may be considered for the decrease of  $V_{\max}$  caused by synthetic polymers. Viscosity due to entry of polymer molecules into the filament lattice might decrease velocity. This effect if present probably does not provide a complete explanation for the changes in velocity shown in Fig. 9 because dextran T-500 is a much larger molecule than PVP-40 and would not be expected to enter the filament lattice as much as PVP-40. Both polymers reduce  $V_{\max}$ . Drag due to passive interactions between the filaments cannot be ruled out, but if present it would not be viscous in nature because the immediate force–extension curves of fibers activated in polymer solution show pure elasticity (Goldman and Simmons, 1986). The buckling hypothesis qualitatively explains the behavior of the force–extension curves (Goldman and Simmons, 1986) as well as the force–velocity curve on compressing the filament lattice. The results are consistent with the hypothesis of Huxley (1957) that  $V_{\max}$  is defined by a balance of positive and negative cross-bridge forces.

I am grateful to Mr. Miles J. Gessow for skillful mechanical and electronic construction, to Mr. Mark A. Luttmann for assistance with the experiments, Dr. L. E. Ford for helpful discussion, and to Star Lab Photo, Narberth, PA, for refined color printing.

The work was supported by National Institutes of Health grants AM-26846 and AM-00745 and by the Muscular Dystrophy Association.

Received for publication 18 August 1986 and in final form 27 February 1987.

## REFERENCES

- Adler, R. 1967. Interaction between light and sound. *IEEE Spectrum*. 4:42-54.
- Altringham, J. D., R. Bottinelli, and J. W. Laktis. 1984. Is stepwise sarcomere shortening an artefact? *Nature (Lond.)*. 307:653-655.
- Born, M., and E. Wolf. 1975. Principles of Optics. Pergamon Press, New York.
- Bragg, W. L. 1933. X-Ray optics. In *The Crystalline State*. Vol. 1: A General Survey. G. Bell and Sons, London. 208-340.
- Brenner, B. 1980. Effect of free sarcoplasmic  $Ca^{2+}$  concentration on maximum unloaded shortening velocity: measurements on single glycerinated rabbit psoas muscle fibres. *J. Muscle Res. Cell Motil.* 1:409-428.
- Brenner, B. 1983. Technique for stabilizing the striation pattern in maximally calcium-activated skinned rabbit psoas fibers. *Biophys. J.* 41:99-102.
- Brenner, B. 1985. Sarcomeric domain organization within single skinned rabbit psoas fibers and its effects on laser light diffraction patterns. *Biophys. J.* 48:967-982.
- Brozovich, F. V., and G. H. Pollack. 1983. Muscle contraction generates discrete sound bursts. *Biophys. J.* 41:35-40.
- Dantzig, J. A., and Y. E. Goldman. 1985. Suppression of muscle contraction by vanadate. Mechanical and ligand binding studies on glycerol-extracted rabbit fibers. *J. Gen. Physiol.* 86:305-327.
- Delay, M. J., N. Ishide, R. C. Jacobson, G. H. Pollack, and R. Tirosh. 1981. Stepwise sarcomere shortening: analysis by high-speed cinematography. *Science (Wash. DC)*. 213:1523-1525.
- Edman, K. A. P. 1979. The velocity of unloaded shortening and its relation to sarcomere length and isometric force in vertebrate muscle fibres. *J. Physiol. (Lond.)*. 291:143-159.
- Ellis, G. W. 1979. A fiber-optic phase-randomizer for microscope illumination by laser. *J. Cell Biol.* 83 (2, Pt. 2):303a. (Abstr.)
- Ferenczi, M. A., Y. E. Goldman, and R. M. Simmons. 1984. The dependence of force and shortening velocity on substrate concentration in skinned muscle fibres from *Rana temporaria*. *J. Physiol. (Lond.)*. 350:519-543.
- Ford, L. E., A. F. Huxley, and R. M. Simmons. 1977. Tension responses to sudden length change in stimulated frog muscle fibres near slack length. *J. Physiol. (Lond.)*. 269:441-515.
- Goldman, Y. E. 1983. The relationship between force and velocity of sarcomere shortening measured by white light diffraction. *Biophys. J.* 41:257a. (Abstr.)
- Goldman, Y. E., M. G. Hibberd, and D. R. Trentham. 1984. Relaxation of rabbit psoas muscle fibres from rigor by photochemical generation of adenosine-5'-triphosphate. *J. Physiol. (Lond.)*. 354:577-604.
- Goldman, Y. E., and R. M. Simmons. 1984. Control of sarcomere length in skinned muscle fibres of *Rana temporaria* during mechanical transients. *J. Physiol. (Lond.)*. 350:497-518.
- Goldman, Y. E., and R. M. Simmons. 1986. The stiffness of frog skinned muscle fibres at altered lateral filament spacing. *J. Physiol. (Lond.)*. 378:175-194.
- Gordon, A. M., A. F. Huxley, and F. J. Julian. 1966. Tension development in highly stretched vertebrate muscle fibres. *J. Physiol. (Lond.)*. 184:143-169.
- Granzier, H. L.M., and G. H. Pollack. 1985. Stepwise shortening in unstimulated frog skeletal muscle fibres. *J. Physiol. (Lond.)*. 362:173-188.
- Gulati, J., and A. Babu. 1984. Intrinsic shortening speed of temperature-jump-activated intact muscle fibers. Effects of varying the osmotic pressure with sucrose and KCl. *Biophys. J.* 45:431-445.
- Huxley, A. F. 1957. Muscle structure and theories of contraction. *Prog. Biophys. Biophys. Chem.* 7:255-318.
- Huxley, A. F., and L. D. Peachey. 1961. The maximum length for contraction in vertebrate striated muscle. *J. Physiol. (Lond.)*. 156:150-165.
- Julian, F. J., and R. L. Moss. 1980. Sarcomere length-tension relations of frog skinned muscle fibres at lengths above the optimum. *J. Physiol. (Lond.)*. 304:529-539.
- Julian, F. J., L. C. Rome, D. G. Stephenson, and S. Striz. 1986. The maximum speed of shortening in living and skinned frog muscle fibres. *J. Physiol. (Lond.)*. 370:181-199.
- Korpel, A., R. Adler, P. Desmares, and W. Watson. 1966. A television display using acoustic deflection and modulation of coherent light. *Proc. IEEE*. 54:1429-1437.
- Matsubara, I., and G. F. Elliott. 1972. X-ray diffraction studies on skinned single fibres of frog skeletal muscle. *J. Mol. Biol.* 72:657-669.
- Matsubara, I., Y. E. Goldman, and R. M. Simmons. 1984. Changes in the lateral filament spacing of skinned muscle fibres when cross-bridges attach. *J. Mol. Biol.* 173:15-33.
- Moss, R. L. 1979. Sarcomere length-tension relations of frog skinned muscle fibres during calcium activation at short lengths. *J. Physiol. (Lond.)*. 292:177-192.
- Pollack, G. H. 1986. Quantal mechanisms in cardiac contraction. *Circ. Res.* 59:1-8.
- Pollack, G. H., T. Iwazumi, H. E. D. J. ter Keurs, and E. F. Shibata. 1977. Sarcomere shortening in striated muscle occurs in stepwise fashion. *Nature (Lond.)*. 268:757-759.
- Rome, L. C., S. Striz, D. G. Stephenson, and F. J. Julian. 1985. The maximum speed of shortening in intact and skinned muscle fibers. *Biophys. J.* 47:289a. (Abstr.)
- Rosenthal, A. H. 1955. Color control by ultrasonic wave gratings. *J. Opt. Soc. Am.* 45:751-756.
- Rüdel, R., and F. Zite-Ferenczy. 1979. Do laser diffraction studies on striated muscle indicate stepwise sarcomere shortening? *Nature (Lond.)*. 278:573-575.
- Rüdel, R., and F. Zite-Ferenczy. 1980. Efficiency of light diffraction by cross-striated muscle fibers under stretch and during isometric contraction. *Biophys. J.* 30:507-516.
- Sundell, C. L., Y. E. Goldman, and L. D. Peachey. 1986. Fine structure in near-field and far-field laser diffraction patterns from skeletal muscle fibers. *Biophys. J.* 49:521-530.